

# NUMERICAL INVESTIGATION OF THE EFFECT OF BIOMIMETIC TUBERCLES ON THE HYDRODYNAMIC RESISTANCE OF A FLAT PLATE

**Alessandro Marino**, Fincantieri S.p.A., Italy & University of Strathclyde, UK  
**Roberto Ravenna**, University of Strathclyde, UK  
**Momchil Terziev**, University of Strathclyde, UK  
**Mehmet Atlar**, University of Strathclyde, UK

*Mimicking the features of living animals or plants is often an efficient solution for engineering problems. In the marine world, humpback whales (*Megaptera Novaeangliae*) are well known for their remarkable agility, despite their bulky bodies, and biologists, as well as engineers, have studied them to uncover their secret. While the tubercles on the leading edge of their pectoral fins have been successfully applied to wing profiles in aeronautics [1, 2] and marine technology [3–5], the present work presents the application of the circular-base tubercles located on the head of these whales to a flat surface. In fact, the circular-base tubercles proved to be effective in manipulating the flow over the flat plate [6–8] and in some cases, also reduced the total drag. In the present study, Computational Fluid Dynamics (CFD) simulations were performed in order to expand the investigation in [6] and replicate the experimental results obtained in [7, 8]. Simulations were run with both RANS and DES solvers, and the results were analysed and compared. The results confirmed the trend observed during the previous experimental campaign, showing that biomimetic tubercles can modify, and in some instances improve, the performance of a flat plate by reducing its drag.*

## 1. Introduction

While shipping is more energy-efficient than air or land transport, reducing ship resistance remains a key concern for naval architects. Around 2.9% of human-made CO<sub>2</sub> emissions are due to international shipping, according to the International Maritime Organisation (IMO) [9]. Even marginal improvements in ship resistance can result in considerable reductions in fuel consumption and emissions. Therefore, the International Towing Tank Conference (ITTC) encourages further research into innovative ways to reduce ship resistance [10].

Biomimetics (the application of biological principles to engineering problems) has historically proven an inexhaustible inspiration and a promising direction to improve ship resistance [11]. Among the best-known examples are the tubercles of the humpback whale (*Megaptera novaeangliae*), rounded protuberances that appear along the leading edge of the pectoral fins and across the head. Tubercles' effectiveness has been demonstrated experimentally and numerically on lifting surfaces, with applications extending from aeronautics to rudders and tidal turbines [5, 12–14] where they have been shown to influence lift, drag, and stall behaviour [15, 16].

While leading-edge tubercles have been extensively studied, the function of the circular-base tubercles found on the head of humpback whales remains less clear. Biological studies have suggested both sensory and hydrodynamic roles [17, 18]. In fluid dynamics contexts, however, these head tubercles have recently attracted interest as potential flow-control features.

The numerical simulations of [6] showed that head tubercles have the potential to modify boundary-layer development on a flat plate. Flat plate resistance with tubercles was examined experimentally in [8], where towing tank tests demonstrated that the hydrodynamic influence of tubercles is strongly dependant on their placement. The findings indicated that tubercles can indeed alter the flow over the

plate and, depending on their placement, lead to either reductions or increases in drag. The results in [8] provided an initial indication that different tubercle configurations might be exploited to improve the hydrodynamic efficiency of flat surfaces. In particular, upstream and downstream rows of tubercles produced measurable reductions in total resistance of the flat plate, up to ~1.8% at high Reynolds numbers, while mid-length or distributed arrangements led instead to drag penalties. Although these experiments provided the first empirical evidence of the effect of head tubercles on a flat plate, they were constrained by the test facility to a velocity range of 1.5-4.5 m/s. Extending the investigation requires numerical modelling, which not only allows the study of higher Reynolds numbers but also offers insight into the flow structures responsible for the observed behaviour.

The present study replicates the experiments of [8] on a flat plate with a Reynolds-Averaged Navier-Stokes (RANS) solver as the baseline approach. A Detached Eddy Simulation (DES) model is also employed in order to examine whether hybrid turbulence approaches provide advantages in capturing the localised vortical structures associated with the tubercles. To the best of the authors' knowledge, a numerical evaluation of the hydrodynamic effects of tubercles on a flat plate and the applicability of CFD for this purpose has not been previously conducted in the context of naval architecture.

The objectives of the work are: (i) to validate the numerical predictions of the effects of tubercles on a flat plate against the existing experimental data; (ii) to assess the suitability of RANS and DES approaches for modelling the flow over 'tubercled' flat plates; and (iii) to extend the analysis to a wider range of velocities than was achievable in the towing tank. In addressing these objectives, this work aims to numerically investigate the effect of biomimetic tubercles on the hydrodynamic resistance of a flat plate.

The structure of this paper is as follows: the Methodology section details the CFD approach and simulation setup used in this study. The Results section presents a validation of the CFD findings against experimental data from [8] and analyses the performance of the RANS and DES solvers. Finally, the conclusions section summarises the key findings and offers recommendations for future work.

## **2. Methodology**

CFD simulations are employed to replicate the experimental results described in [8] and subsequently extend the velocity range that was achievable in the Towing Tank of the University of Strathclyde (UoS)'s Kelvin Hydrodynamics Laboratory (KHL) [19]. The Experimental Fluid Dynamics (EFD) tests were performed by towing a submerged flat steel plate at different speeds (1.5 m/s to 4.5 m/s, with 0.5 m/s steps). Different configurations of tubercles were attached to both sides of the plate. Both RANS and DES simulations were used to simulate the experiments. The RANS model was first tested and validated, and then its settings served as the basis for the DES simulations.

### **2.1. Geometry**

The flat panel and the tubercles are modelled exactly as the ones tested during the experimental campaign. The flat plate has a rectangular shape and presents a rounded leading edge ( $r = 2.5$  mm) and a sharp trailing edge. The plate is 1490 mm long and 800 mm wide, with a thickness of 5 mm. The plate is towed longitudinally, submerged at a draught of 586 mm.

Four tubercle distribution configurations are tested, in accordance with [6, 8], which are: no tubercles (reference panel) and tubercles located at the upstream, mid-length, and downstream positions. The 'Distributed' configuration is not considered in the present paper, and seven tubercles are applied in a vertical row, covering the relative area on the plate. Each tubercle is axisymmetric and has a sinusoidal profile, measuring 74 mm in length and 10 mm in height. The vertical rows cover the whole depth of the plate, from the free surface to the bottom. Fig. 1 shows the plate with tubercles used for the experimental campaign.

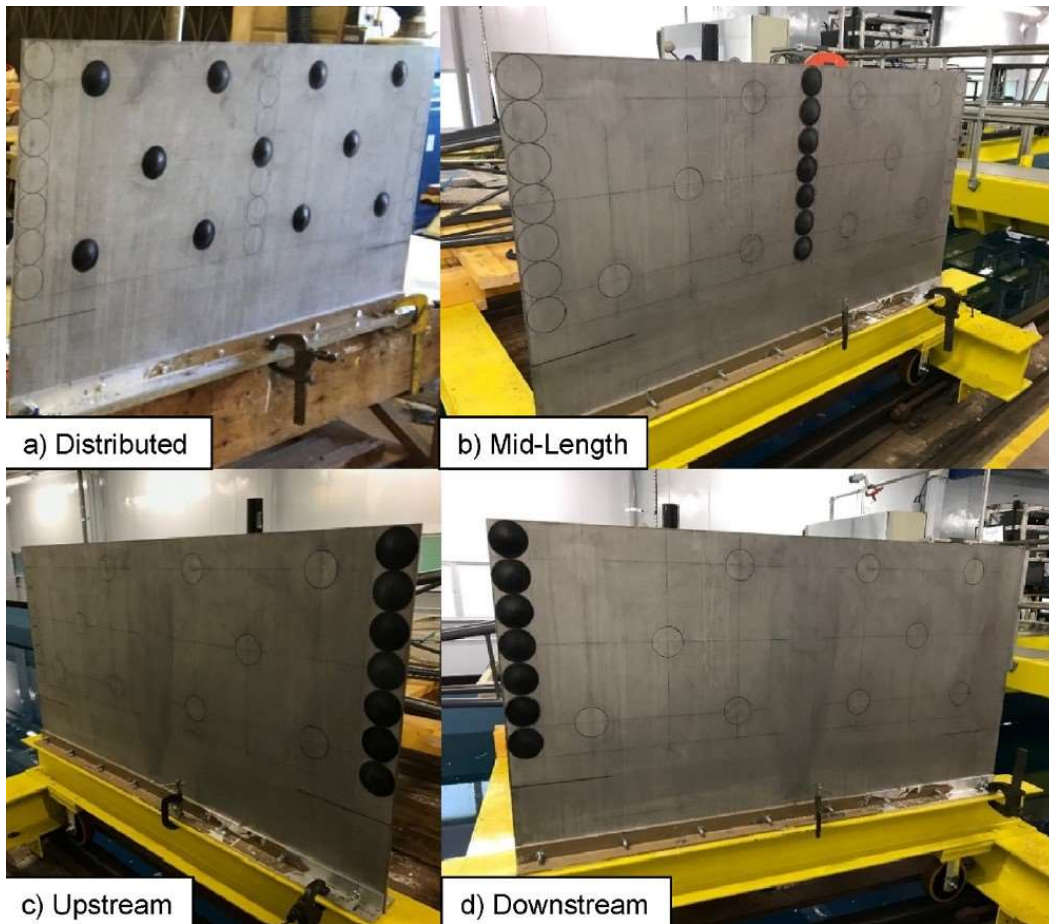


*Fig. 1- Plate with tubercles configurations tested in [8]*

The simulation domain extends from 2 plate lengths upstream to 4 lengths downstream, while depth and width resemble those of KHL's towing tank, i.e. 2500 mm and 2300 mm, respectively. Above the free surface, the domain is extended to 1.5 plate lengths. Fig. 2 shows the computational domain.

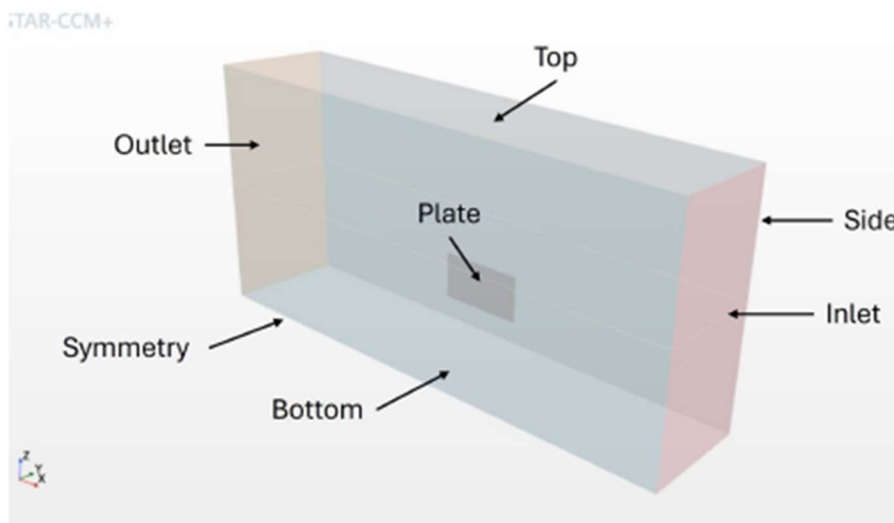


*Fig. 2 - Computational domain*

## 2.2. Numerical simulations setup

Similarly to [6], a Shear Stress Transport (SST)  $k-\omega$  turbulence model is adopted. The domain is divided into a trimmed mesh with a thin prism layer, whose thickness is set parametrically, ensuring that the  $y^+$  value near the plate surface is always equal to 10. This value was chosen after a series of tests with increasing  $y^+$ , from 1 to 50, as it best replicated the experimental results. The only exception is the upstream configuration, where it is found that a  $y^+$  equal to 5 is necessary to capture the phenomena in the region where the flow is still laminar. In this configuration, a volume mesh refinement is applied to locally reduce the mesh size to 1.75 mm.

Two volume mesh refinements are applied on the free surface: one spanning vertically from -15 mm to +15 mm, the second from -30 mm to +30 mm. The former (inner refinement) reduces the vertical dimension of the cells to 1.75 mm, while the latter (outer refinement) reduces it to 3.5 mm. Finally, two further volume refinements are set to properly model the Kelvin wake area. The first extends 1.5 plate lengths downstream of the panel and, vertically, from -50 mm to 50 mm. The second extends 2.3 lengths downstream and from -75 mm to 75 mm along the vertical direction. The inner Kelvin wake refinement locally reduces the cell size to 7 mm (3.5 mm in the vertical direction); the outer Kelvin wake refinement sets the local cell size to 28 mm. Fig. 3 shows a detail of the mesh.

An implicit unsteady solver is employed, and the time step is chosen to maintain a Courant number of approximately 1 near the plate surface. The domain's faces of all simulations are treated as walls, while a symmetry plane is placed longitudinally along the entire domain to halve the number of necessary cells, thereby reducing computational time. Finally, the water density and dynamic viscosity are  $998.778 \text{ kg/m}^3$  and  $1.08 \times 10^{-3} \text{ Pa}\cdot\text{s}$ , respectively.

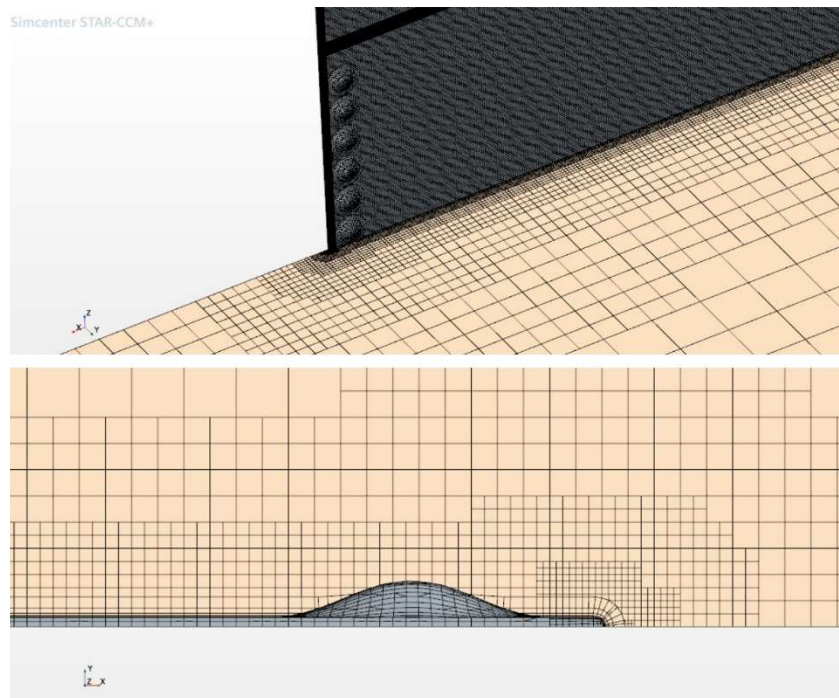


*Fig. 3 - Domain mesh on Upstream configuration: perspective view (top) and top view (bottom)*

The mesh settings described above are also used to set up the DES simulations, which employ an SST (Menter)  $k-\omega$  Detached Eddy turbulence model with a second-order convection scheme. DES simulations are performed only on the tubercle configurations. The results obtained with both turbulence models are compared to the experimental values and serve as a starting point for extending the velocity range.

### 3. Results

This section describes the steps taken to achieve the numerical results, specifically the grid dependency analysis on the reference flat plate and all tubercle configurations, as well as the  $y^+$  variation analysis on the flat plate. Finally, the CFD results are compared to the experimental ones, within their velocity range, and between the two turbulence models within the extended range.

#### 3.1. Grid dependency and $y^+$ variation analysis

The grid dependency test is initially run on the Reference configuration and subsequently on all the tubercle configurations, at both ends of the experiments' velocity range, i.e., 1.5 m/s and 4.5 m/s. The adopted procedure is described in [20] and is based on the findings presented in [21]. Three mesh sizes are chosen, namely Coarse, Medium and Fine, and the total resistance  $R_t$  of the plate is employed as the comparison parameter  $\phi$ . The final Grid Convergence Index (GCI) is reported in Table 1 below, together with the number of mesh cells for all the configurations (N) and the  $\phi$  values.

*Table 1 - Grid dependency analysis*

	<b>Reference at 1.5 m/s</b>	<b>Reference at 4.5 m/s</b>	<b>Downstream at 1.5 m/s</b>	<b>Downstream at 4.5 m/s</b>
$N_f$	4837274	4848498	4840595	4852601
$N_m$	2500353	2183667	2145863	2190528
$N_c$	1198965	1195113	1195125	1196565
$R_t$ (fine mesh)	8.55 N	65.50 N	8.80 N	65.44 N
$R_t$ (medium mesh)	8.49 N	67.06 N	8.66 N	66.27 N
$R_t$ (coarse mesh)	9.08 N	70.93 N	9.08 N	69.55 N
GCI	0.143 %	0.982 %	0.648 %	0.265 %
	<b>Mid-length at 1.5 m/s</b>	<b>Mid-length at 4.5 m/s</b>	<b>Upstream at 1.5 m/s</b>	<b>Upstream at 4.5 m/s</b>
$N_f$	4838939	4845358	4841437	4845854
$N_m$	2509632	2192191	2142555	2182533
$N_c$	1195698	1196230	1192870	1193884
$R_t$ (fine mesh)	9.04 N	69.20 N	9.09 N	67.16 N
$R_t$ (medium mesh)	8.90 N	70.45 N	9.10 N	68.19 N
$R_t$ (coarse mesh)	9.53 N	74.07 N	9.43 N	71.93 N
GCI	0.652 %	0.608 %	0.002 %	0.364 %

For the accuracy of prediction, the fine mesh is chosen for all simulations, even though the  $GCI < 1\%$  indicates a reliable independence of the results from the grid size.

Subsequently, an analysis of the variation in the average  $y^+$  value on the plate surface is performed on the reference plate, within a range spanning from 1 to 50, across the entire experimental speed range. The average  $y^+$  and the average  $R_t$  percentage difference, compared to the experimental values, are reported in Table 2.

*Table 2 -  $y^+$  variation analysis on the Reference configuration*

Average $y^+$	1	10	30	50
Average absolute $R_t$ difference	15.4 %	1.9 %	4.5 %	6.6 %

A  $y^+$  value of 10 is chosen for the final mesh setup. Although such a value is usually not recommended for RANS simulations, it is deemed acceptable due to its coherence with the experimental results and the nature of the addressed turbulent phenomenon, which can lead to unstable results in this type of simulation. The same setup is then employed to replicate the empirical results on the plate with

tubercles in the three configurations. The only exception is the Upstream configuration, where a  $y^+$  value of 5 on the plate surface yields results more consistent with the experiments.

### 3.2. Presentation of the numerical results

The CFD results are first compared to the experimental data for both turbulence models. The Figures in this section show these comparisons, both in dimensional ( $R_t$ ) and nondimensional forms; the latter shows the total resistance coefficient ( $C_t$ ) of the plates versus the Reynolds number ( $R_e$ ), which are obtained as follows:

$$C_t = \frac{R_t}{\frac{1}{2}\rho S V^2} \quad (1)$$

$$R_e = \frac{VL}{\nu} \quad (2)$$

where  $\rho$  is the water density,  $S$  is the plate's surface area,  $V$  is the towing speed,  $L$  is the plate's length, and  $\nu$  is the water kinematic viscosity.

Fig. 4 to Fig. 11 show the results of the RANS simulations. The maximum percentage difference in the total resistance data is 6.62%, measured at a velocity of 1.5 m/s, for the Reference configuration. Overall, the average difference between the RANS and EFD results is below 2%.

Fig. 12 to Fig. 17, on the other hand, compare the EFD data with the DES simulation results. In this case, the maximum deviation from the experimental data is 9.44%, measured at a velocity of 1.5 m/s, for the Upstream configuration. Overall, the average difference between the DES and EFD results is approximately 2%, with a slightly higher value for the Upstream configuration.

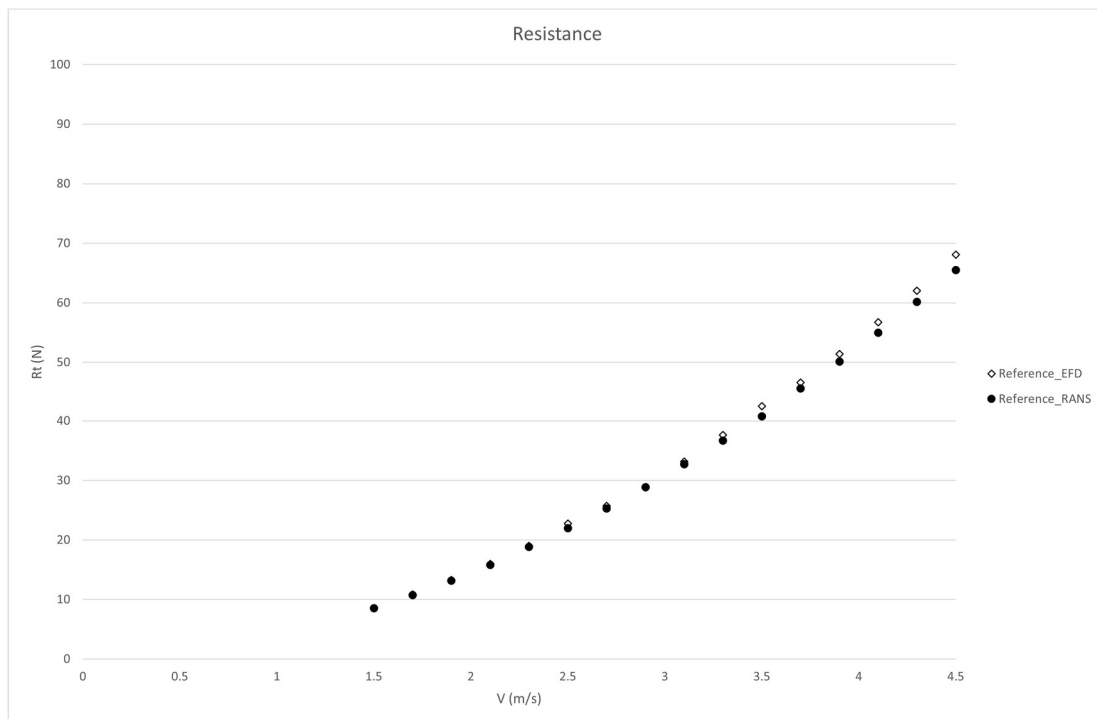
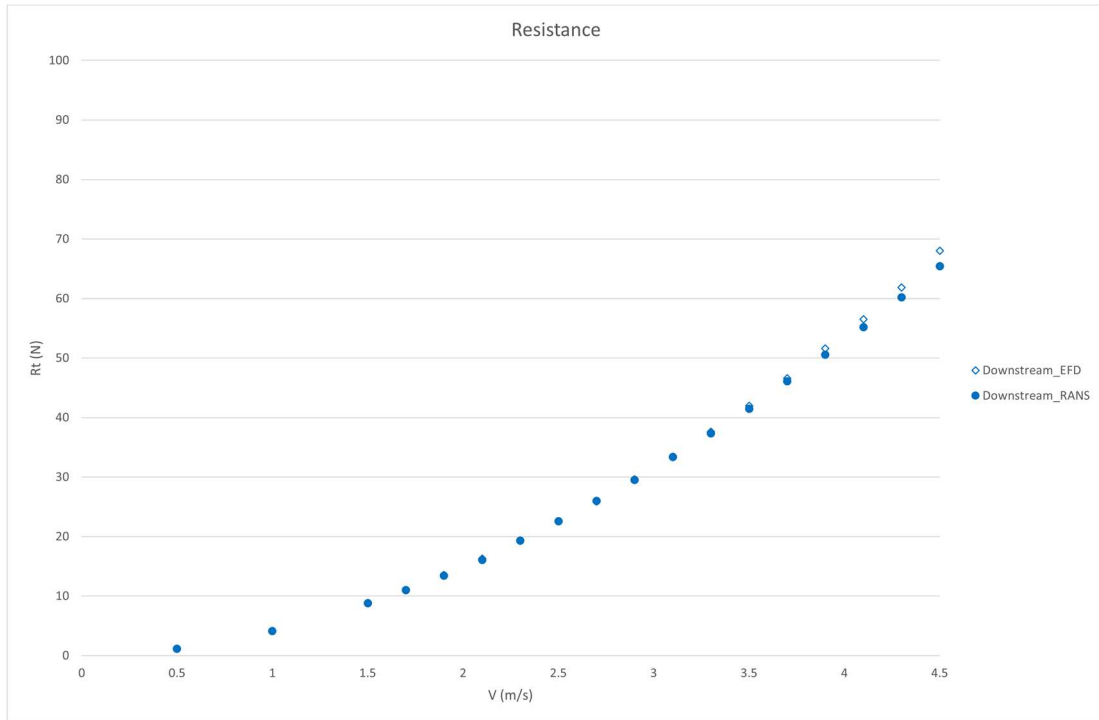
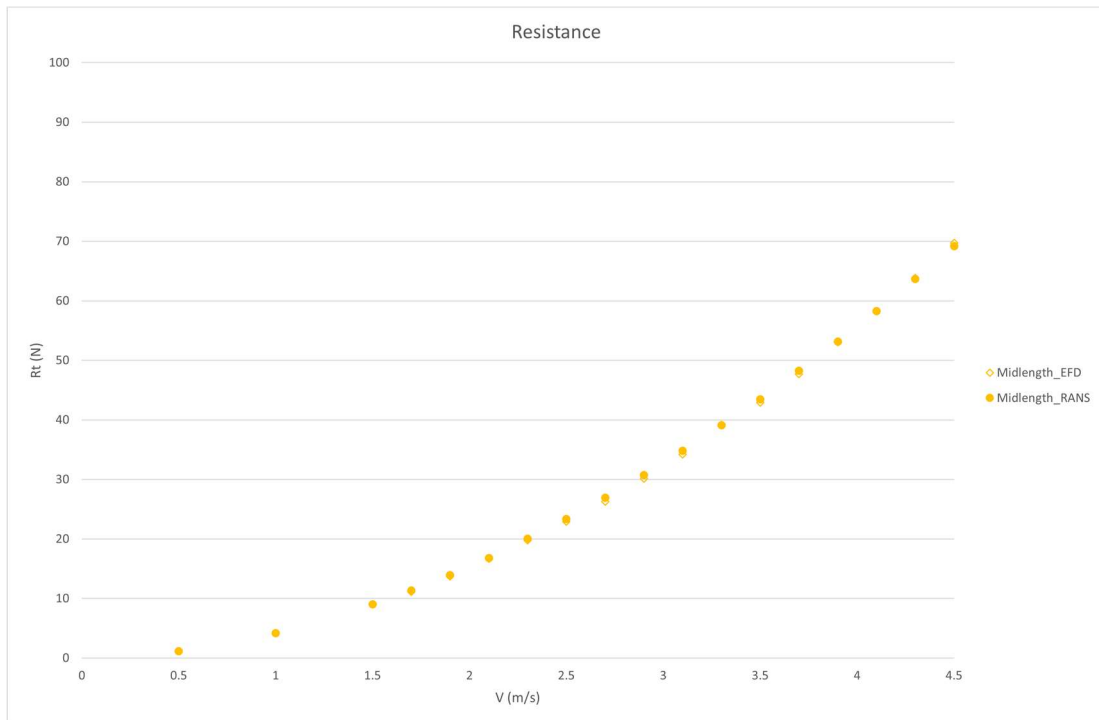


Fig. 4 - Reference configuration  $R_t$  comparison (RANS vs experiments)



*Fig. 5 - Downstream configuration  $R_t$  comparison (RANS vs experiments)*



*Fig. 6 - Midlength configuration  $R_t$  comparison (RANS vs experiments)*

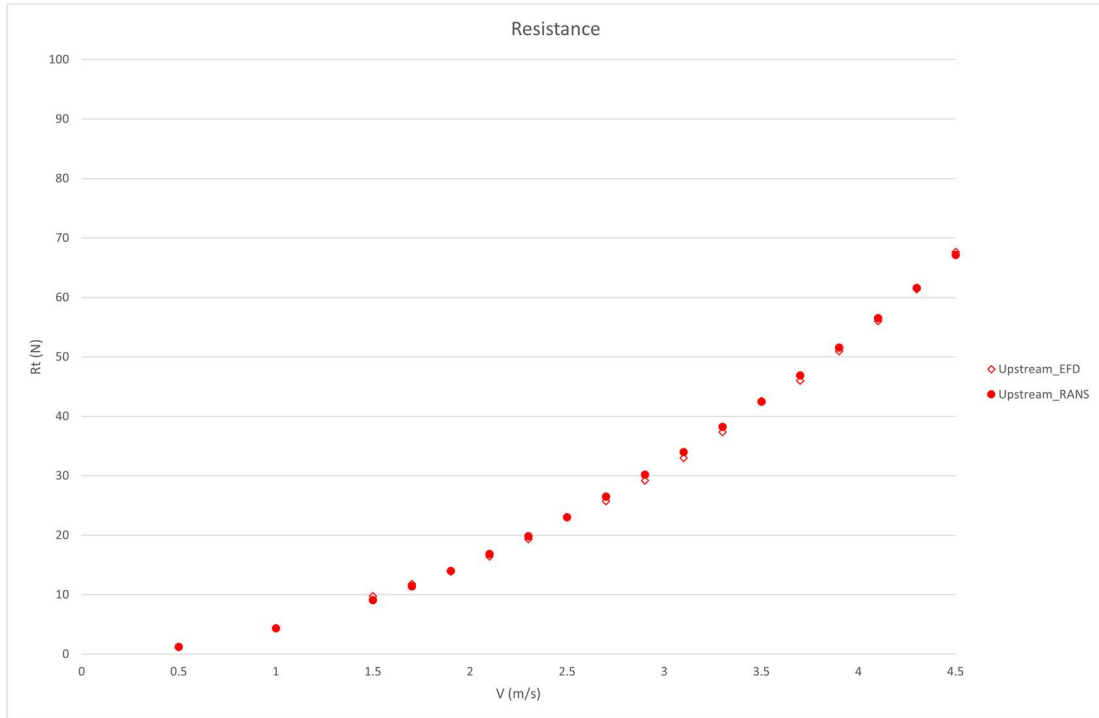


Fig. 7 - Upstream configuration  $R_t$  comparison (RANS vs experiments)

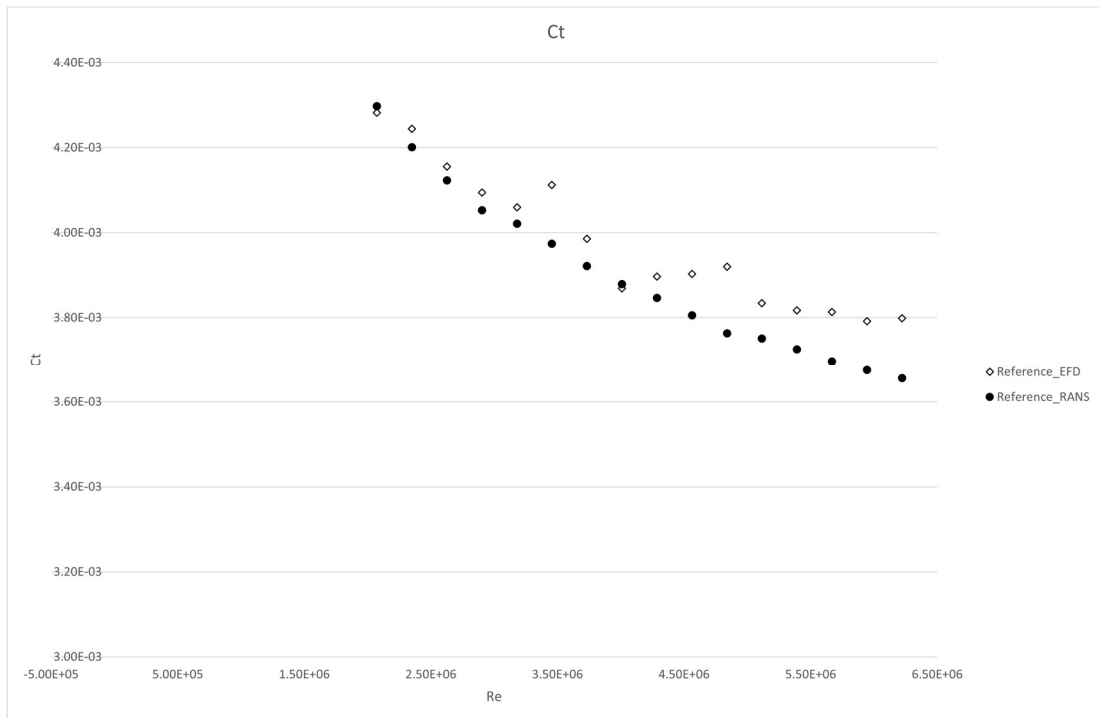


Fig. 8 - Reference configuration  $C_t$  comparison (RANS vs experiments)

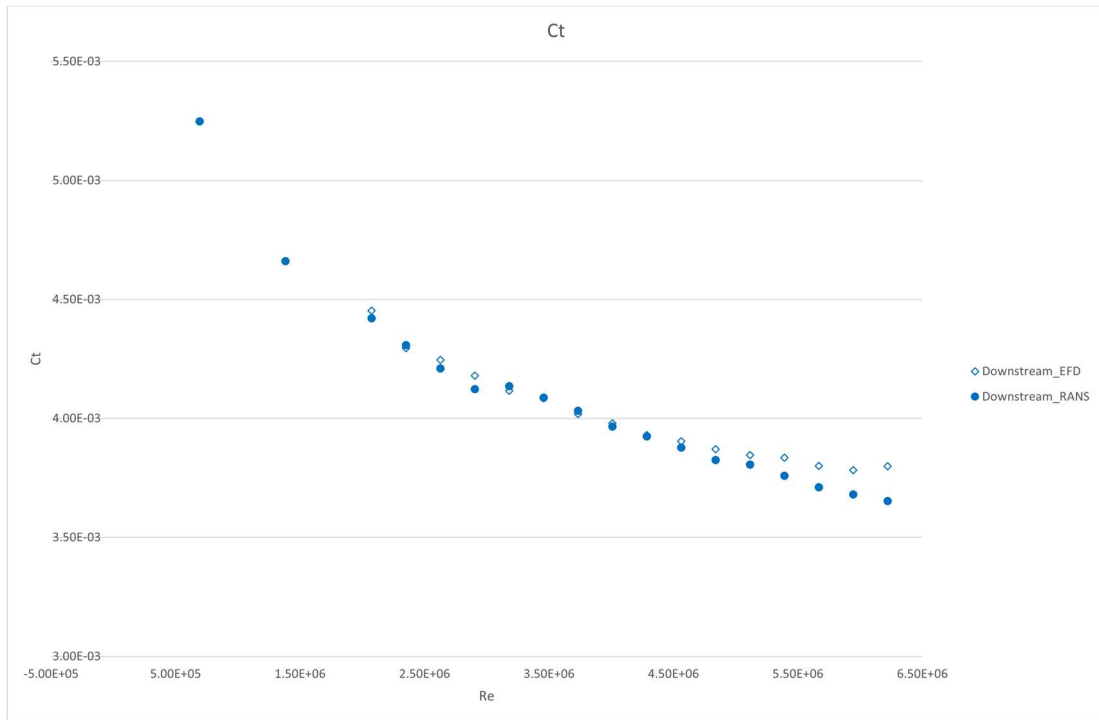


Fig. 9 - Downstream configuration  $C_t$  comparison (RANS vs experiments)

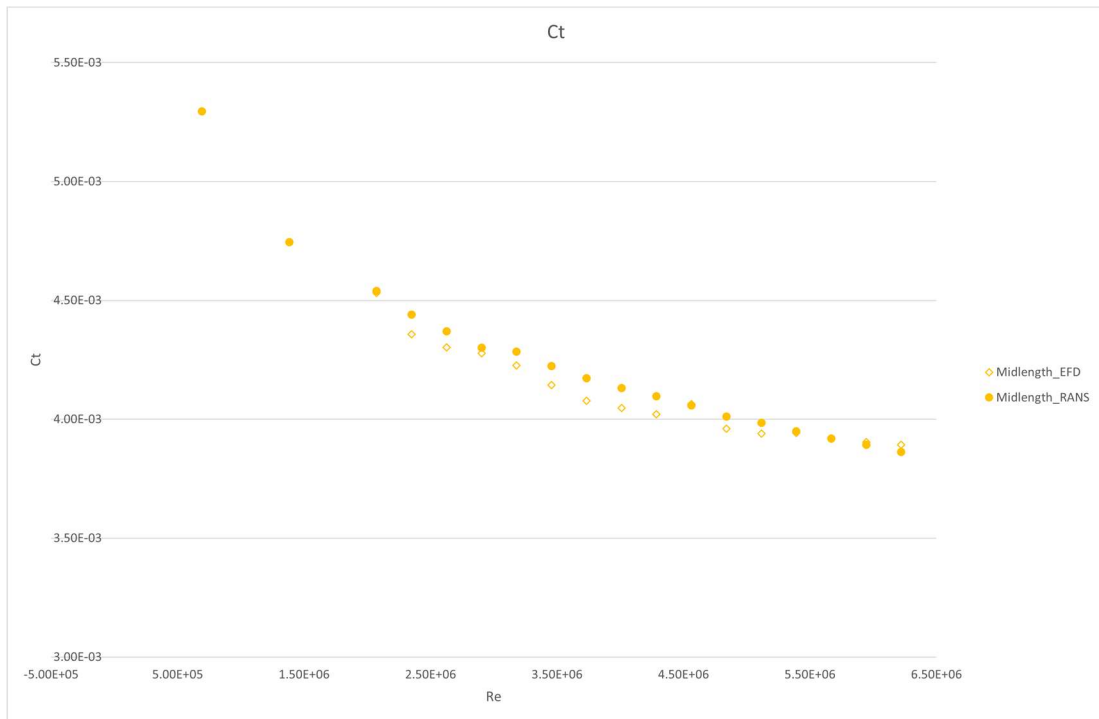


Fig. 10 - Midlength configuration  $C_t$  comparison (RANS vs experiments)

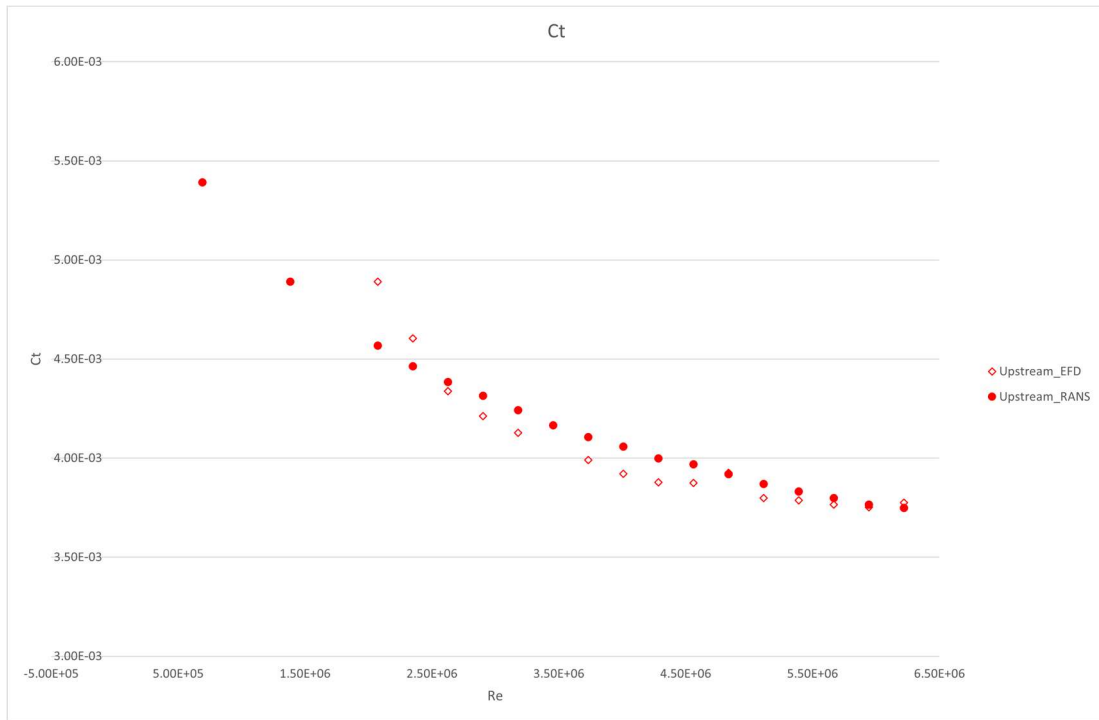


Fig. 11- Upstream configuration  $C_t$  comparison (RANS vs experiments)

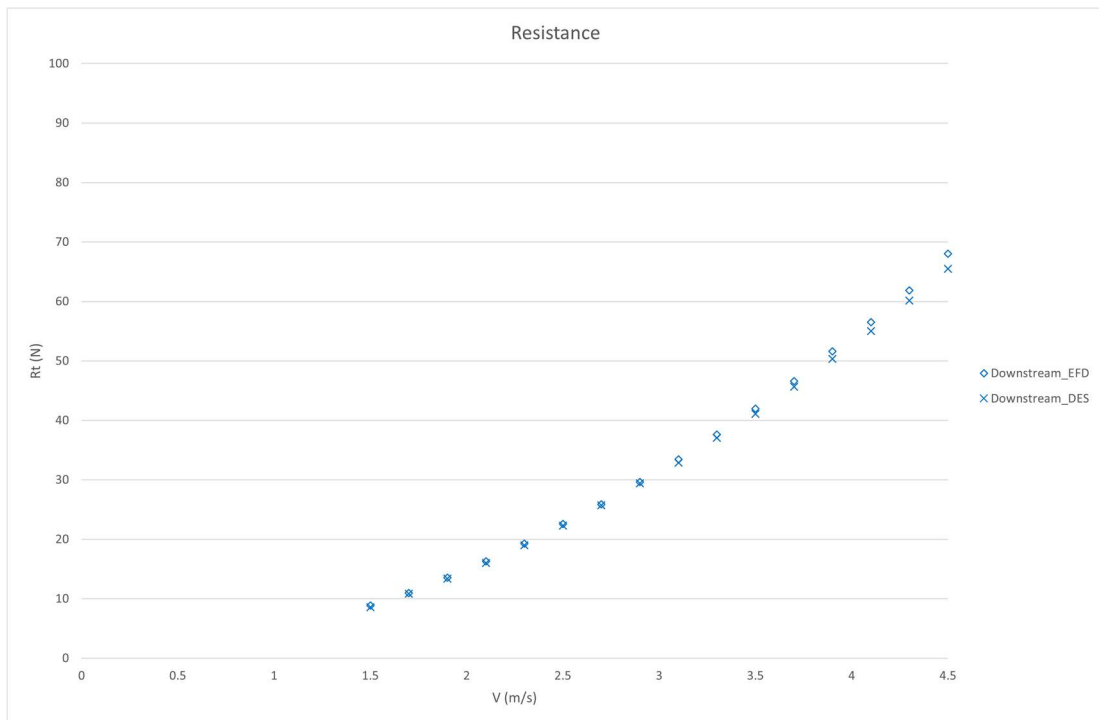


Fig. 12 - Downstream configuration  $R_t$  comparison (DES vs experiments)

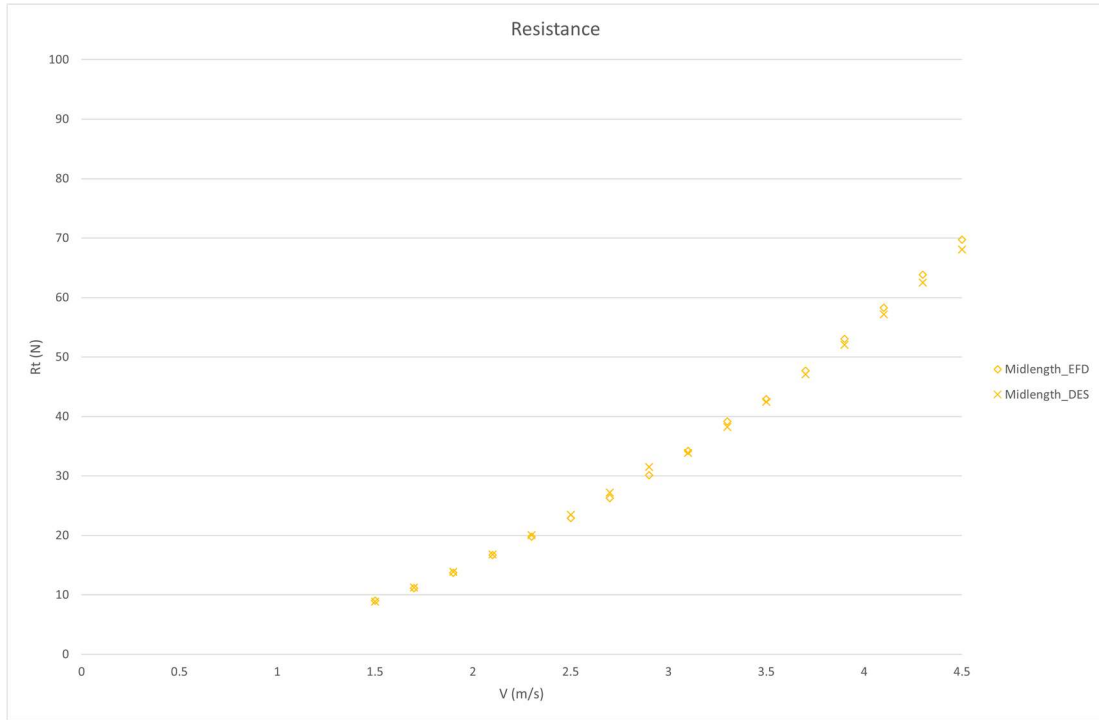


Fig. 13 – Mid-length configuration  $R_t$  comparison (DES vs experiments)

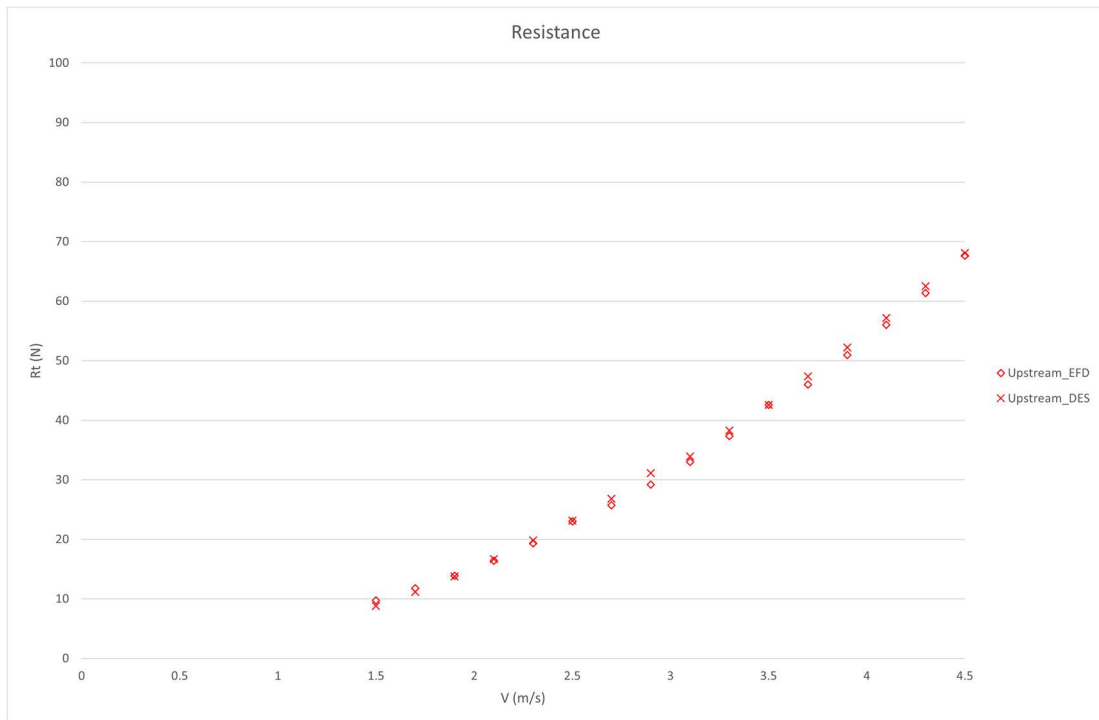


Fig. 14 - Upstream configuration  $R_t$  comparison (DES vs experiments)

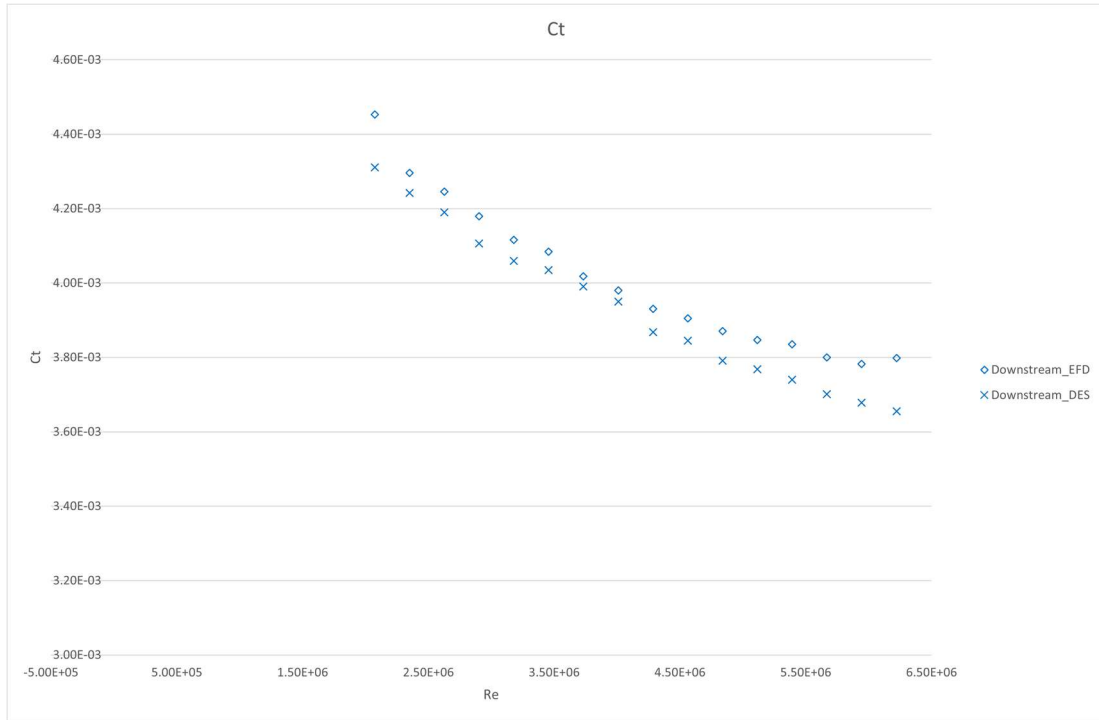


Fig. 15 - Downstream configuration  $C_t$  comparison (DES vs experiments)

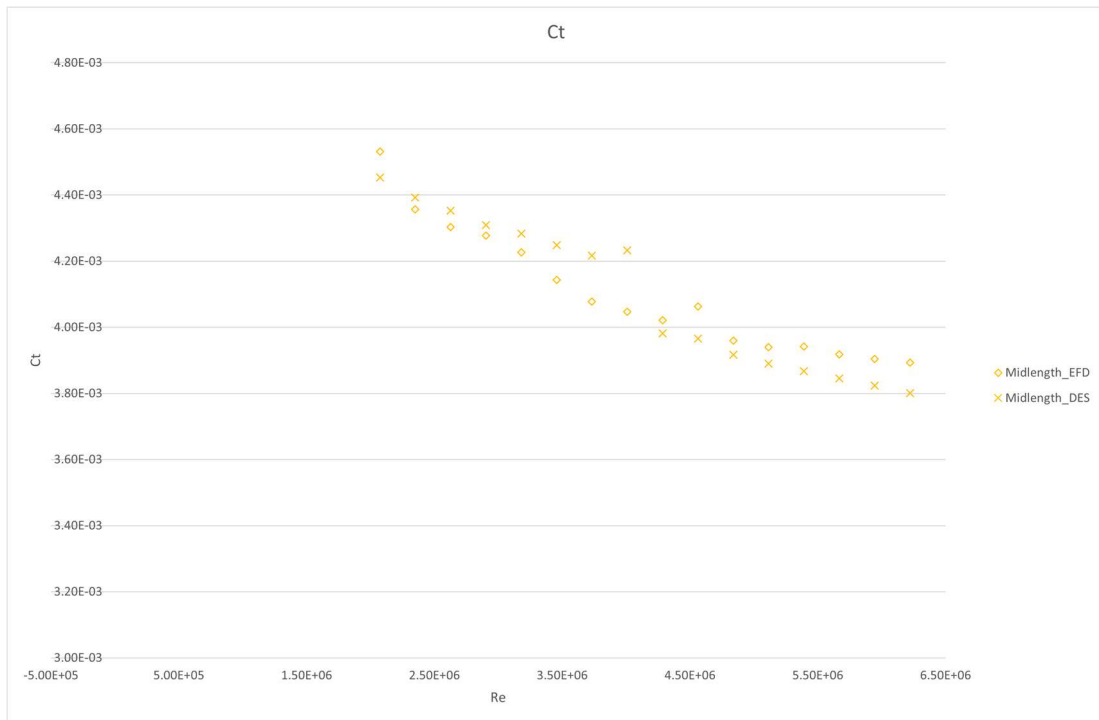
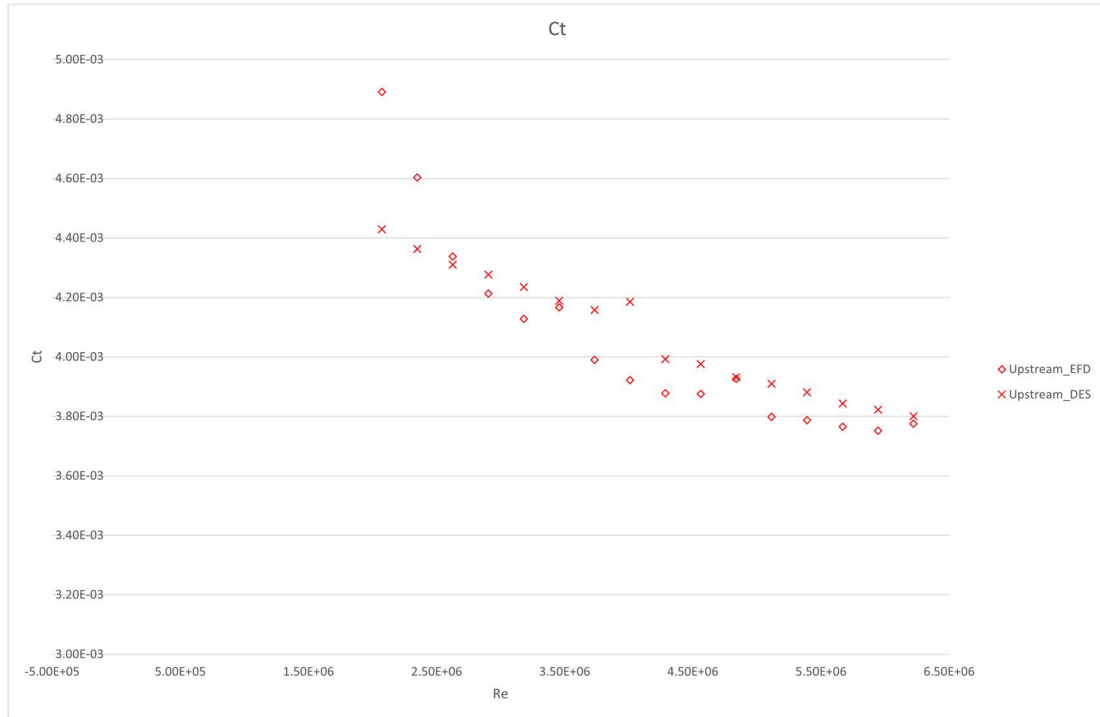


Fig. 16 - Mid-length configuration  $C_t$  comparison (DES vs experiments)



*Fig. 17 - Upstream configuration  $C_t$  comparison (DES vs experiments)*

As the figures above show, the nondimensional values exhibit higher differences in the datasets, while the measured  $R_t$  values show a better resemblance. Additionally, while the results in [8] are presented in  $C_t$  form, the scatter in the nondimensional form may make data interpretation more difficult; hence, the more regular trends shown by the raw  $R_t$  data are preferred for the present analysis.

Finally, both CFD methods are applied to the velocity range expansion, with the results shown in Fig. 18 to Fig. 20.

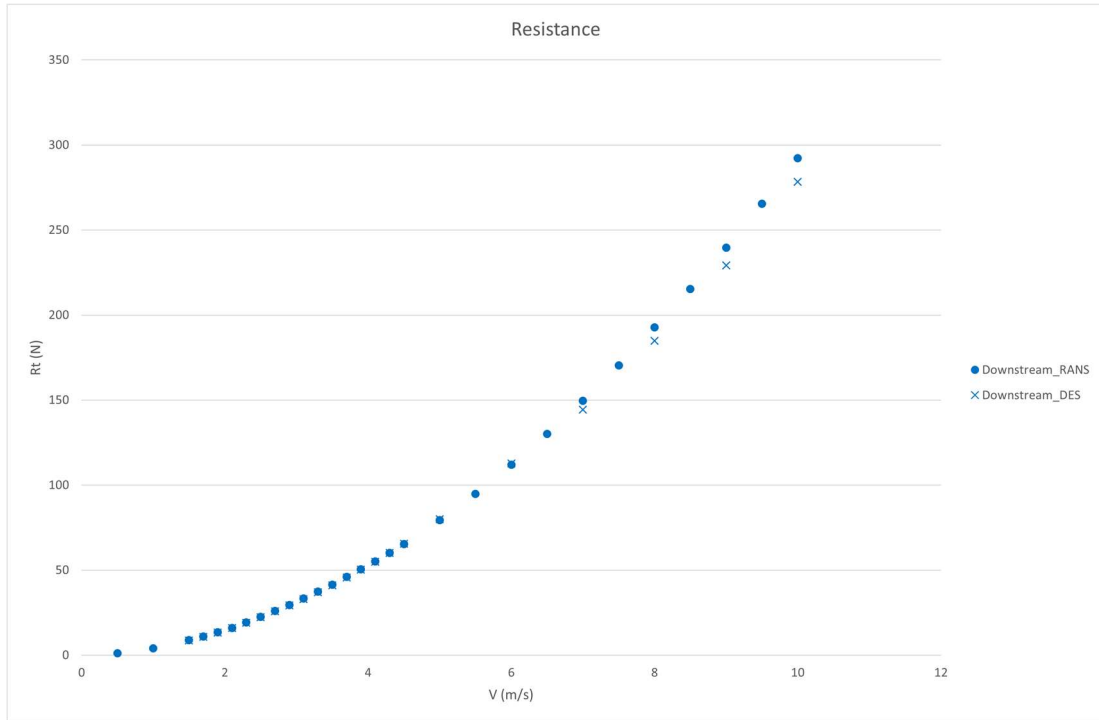


Fig. 18 - Downstream configuration  $R_t$  comparison (RANS vs DES)

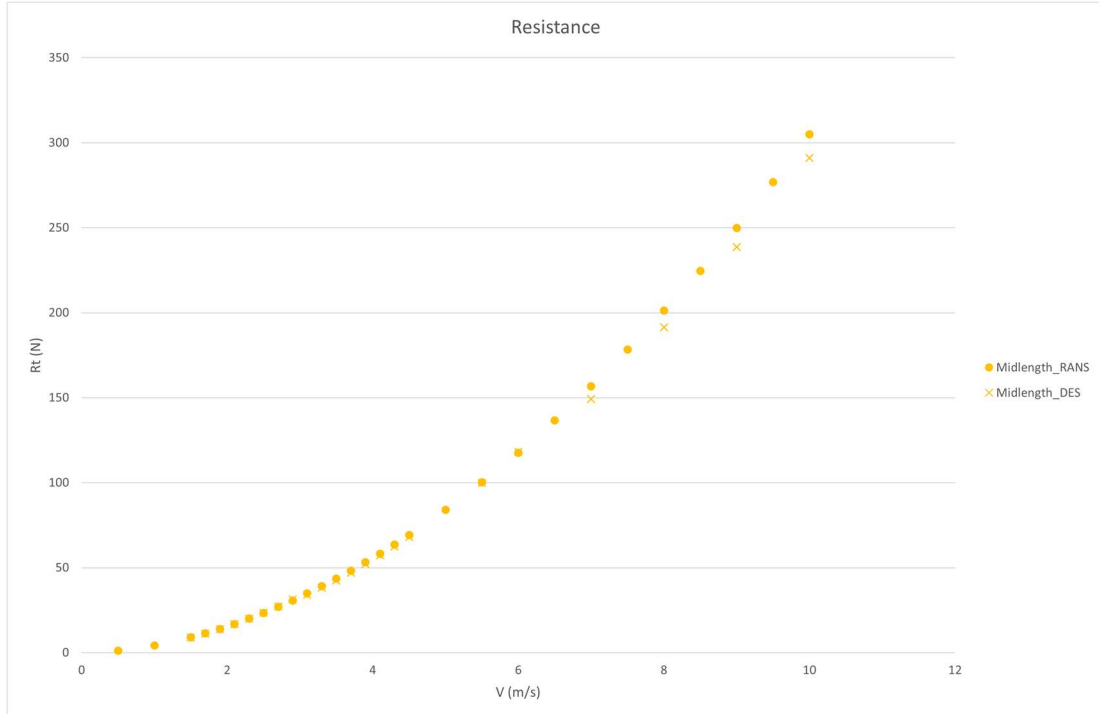


Fig. 19 - Mid-length configuration  $R_t$  comparison (RANS vs DES)

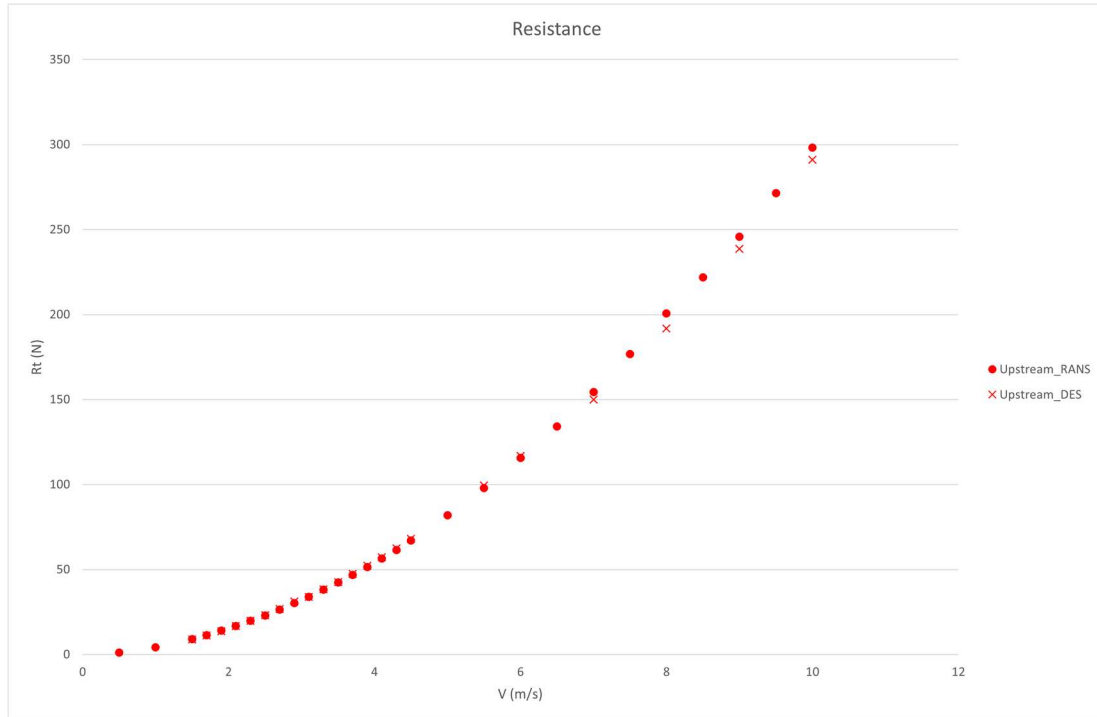


Fig. 20 - Upstream configuration  $R_t$  comparison (RANS vs DES)

Based on the investigation of the results from three configurations, the two turbulence models are comparable within the experimental velocity range (differences of less than 3%), with the gap arising when this range is expanded, especially when the towing speeds exceed 6 m/s. At higher speeds, the DES method yields lower resistance results, with a maximum of -4.85% calculated for the Mid-length configuration at 8 m/s.

Despite these differences, both methods yielded sensible results compared to the EFD values, thereby proving this simulation setup to be a valuable tool for predicting the performance of the 'tubercled' plates.

The RANS simulations proved to be the preferable choice, as they are less computationally demanding and do not compromise the accuracy of the results. On the other hand, one can infer from this comparison that the turbulent phenomena caused by the tubercles are very localised, hence a DES method is not sufficient to fully describe them.

#### 4. Conclusions

The present work aimed at analysing the effect of biomimetic tubercles on a flat plate towed in calm water. This was achieved by replicating EFD results with an RANS and a DES model. The numerical results were validated against empirical data, and the velocity range was extended using the two CFD models. Finally, the two sets of numerical results were compared.

Both CFD models yielded satisfactory results within the experimental velocity range; the differences between the two sets were higher at greater velocities, with the DES data showing a lower resistance prediction. The RANS simulations proved to be a more viable choice for reproducing the effect of tubercles on a flat plate, due to their higher adherence to the EFD data and reduced computational time.

An expansion of the experimental velocity range is encouraged for further validation of the numerical work. At the same time, the use of different CFD models, such as Large Eddy Simulation (LES) or

Direct Numerical Simulation (DNS) can be employed to more accurately model the local phenomena occurring in the very near field of the tubercles.

## Acknowledgements

The CFD simulations performed for the present work were obtained using the commercial code Simcenter STAR-CCM+ with ARCHIE-WeSt High Performance Computer [22] based at the University of Strathclyde.

## 5. References

1. A. Dobre, H. Hangan, B. J. Vickery, 2006, Wake Control Based on Spanwise Sinusoidal Perturbations. *AIAA Journal* **44**, 485–492 (2006).
2. M. D. Bolzon, 2015, Tubercles and their applications. *J Aerosp Eng* **29**, 4015013 (2015).
3. P. Weber, L. Howle, M. M. Murray, 2010, Lift, Drag, and Cavitation Onset On Rudders With Leading-edge Tubercles. *Mar. Technol. Sname News* **47**, 27–36 (2010).
4. F. E. Fish, P. W. Weber, M. M. Murray, E. H. Laurens, 2011, The tubercles on humpback whales' flippers: application of bio-inspired technology. *Integr Comp Biol* **51**, 203 (2011).
5. W. Shi, M. Atlar, R. Norman, 2017, Detailed flow measurement of the field around tidal turbines with and without biomimetic leading-edge tubercles. *Renew Energy* **111**, 688–707 (2017).
6. A. Marino, M. Atlar, Y. K. Demirel, 2019, An investigation of the effect of biomimetic tubercles on a flat plate in *Proceedings of the International Conference on Offshore Mechanics and Arctic Engineering - OMAE*, (2019).
7. R. Ravenna, *et al.*, 2019, Experimental investigation on the effect of biomimetic tubercles on the hydrodynamics of a flat plate in (2019).
8. R. Ravenna, *et al.*, 2022, Experimental study on the effect of biomimetic tubercles on the drag of a flat plate. *Ocean Engineering* **255**, 111445 (2022).
9. IMO, 2020, Fourth Greenhouse Gas Study. (2020).
10. ITTC, 2024, "ITTC-Recommended Procedures and Guidelines."
11. J. F. V. Vincent, O. A. Bogatyreva, N. R. Bogatyrev, A. Bowyer, A.-K. Pahl, 2006, Biomimetics: its practice and theory. *J R Soc Interface* **3**, 471 (2006).
12. P. W. Weber, L. E. Howle, M. M. Murray, F. E. Fish, 2009, Lift and drag performance of odontocete cetacean flippers. *Journal of Experimental Biology* **212**, 2149–2158 (2009).
13. Michael. D. Bolzon, R. M. Kelso, M. Arjomandi, 2016, Tubercles and Their Applications. *J Aerosp Eng* **29**, 04015013 (2016).
14. W. Shi, *et al.*, 2016, Hydrodynamic performance evaluation of a tidal turbine with leading-edge tubercles. *Ocean Engineering* **117**, 246–253 (2016).
15. D. S. Miklosovic, M. M. Murray, L. E. Howle, F. E. Fish, 2004, Leading-edge tubercles delay stall on humpback whale (*Megaptera novaeangliae*) flippers. *Physics of Fluids* **16**, L39–L42 (2004).
16. F. E. Fish, P. W. Weber, M. M. Murray, L. E. Howle, 2011, The tubercles on humpback whales' flippers: Application of bio-inspired technology. *Integr Comp Biol* **51**, 203–213 (2011).
17. E. Mercado, 2014, Short Note: Tubercles: What Sense Is There? *Aquat Mamm* **40**, 95–103 (2014).
18. P. J. Clapham, 2018, Humpback Whale: *Megaptera novaeangliae*. *Encyclopedia of Marine Mammals* 489–492 (2018). <https://doi.org/10.1016/B978-0-12-804327-1.00154-0>.
19. Kelvin Hydrodynamics Laboratory, Kelvin Hydrodynamics Laboratory. Available at: <https://www.strath.ac.uk/engineering/navalarchitectureoceanmarineengineering/workingwithbusinessorganisations/ourfacilities/kelvinhydrodynamicslaboratory/> [Accessed 17 November 2024].

20. I. Celik, U. Ghia, P. Roache, Christopher, 2008, Procedure for estimation and reporting of uncertainty due to discretization in {CFD} applications. *Journal of fluids {Engineering-Transactions} of the {ASME}* **130** (2008).
21. L. F. Richardson, R. T. Glazebrook, 1911, IX. The approximate arithmetical solution by finite differences of physical problems involving differential equations, with an application to the stresses in a masonry dam. *Philosophical Transactions of the Royal Society of London. Series A, Containing Papers of a Mathematical or Physical Character* **210**, 307–357 (1911).
22. ARCHIE-WeSt High Performance Computer. Available at: <https://www.archie-west.ac.uk/> [Accessed 8 September 2025].